engineering proceedings

MDPI

Proceeding Paper

Optimization of Rocker–Bogie Suspension System for Robustness Improvement of Autonomous Rover by Numerical Simulations for Irregular Surfaces in Precision Agriculture †

Leandro Llontop * and Nain M. Ramos

Control Automático y Mecatrónica Inteligente (CAMI), Mechatronics Engineering Program, Faculty of Mechanical Engineering, Universidad Nacional de Ingeniería, Lima 15333, Peru; nramosa@uni.edu.pe

* Correspondence: marco.llontop.h@uni.pe

† Presented at the III International Congress on Technology and Innovation in Engineering and Computing, Lima, Peru, 20–24 November 2023.

Abstract: Mobile robots are capable of moving in various environments and performing complex tasks. They are essential in applications such as planetary exploration, search missions, hazardous waste cleanup, and process automation. Therefore, their study and improvement are relevant today. In this research, we propose optimizing the rocker–bogie suspension system to enhance the robustness of an autonomous rover used in precision agriculture (PA). PA aims to maximize agricultural efficiency and productivity through advanced technologies, and autonomous rovers play a crucial role in enabling real-time data collection and decision-making. This work was developed by implementing numerical simulations to evaluate the performance of the suspension system. The rocker–bogie suspension system is widely used in space exploration as it can avoid obstacles and maintain stability in challenging terrain. Using degrees of freedom and structural analysis, we designed and validated a rocker–bogie-type suspension geometry adapted to the needs of PA. The results of the simulations showed that optimizing the rocker–bogie suspension system significantly improves the rover's robustness on uneven surfaces. The performance of the system was evaluated in various scenarios and conditions through numerical simulations, which supported its feasibility and effectiveness in PA. In conclusion, optimizing the rocker–bogie suspension system is an effective strategy to enhance the robustness of an autonomous rover in PA, as demonstrated by the results of the static simulations. This finding has significant implications for maximizing efficiency and agricultural productivity in PA.

Keywords: rocker–bogie suspension; optimization; robustness; autonomous rover; precision agriculture (PA)

check for updates

Academic Editor: Luis Olivera-Montenegro

Published: 23 January 2025

Citation: Llontop, L.; Ramos, N.M. Optimization of Rocker–Bogie Suspension System for Robustness Improvement of Autonomous Rover by Numerical Simulations for Irregular Surfaces in Precision Agriculture. *Eng. Proc.* **2025**, *83*, 20. https://doi.org/10.3390/engproc2025083020

Copyright: © 2025 by the authors. Licensee MDPI, Basel, Switzerland. This article is an open access article distributed under the terms and conditions of the Creative Commons Attribution (CC BY) license (https://creativecommons.org/licenses/by/4.0/).

1. Introduction and Problematic

The English word "rover" means vagabond, alluding to its main function of exploring celestial bodies. The history of rovers dates back to the 1990s, when NASA launched the first autonomous wheeled rover to Mars, called Sojourner [1]. Since then, NASA has sent several rovers to Mars, including Spirit, Opportunity, Curiosity, and Perseverance (Figure 1). These rovers were designed to explore the surface of the red planet, collect data, take photographs, search for signs of life, and study its geology. The rovers have become crucial tools for space exploration, allowing scientists to deepen knowledge about our solar system and the universe.

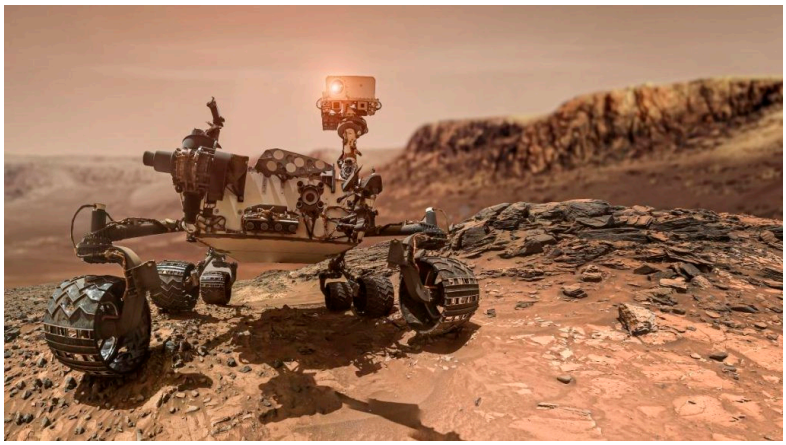


Figure 1. Perseverance, the robotic rover searching for life on Mars. Source: [2].

Although initially designed for aerospace applications, rovers can find applications on Earth, especially in the field of agriculture, where robotics is constantly developing. In recent years, robots capable of performing various agricultural tasks, such as planting, irrigation, harvesting, and pruning, have been developed. For example, Agrobot's E-Series robot shown in Figure 2, with 24 robotic arms and an image recognition algorithm, gently picks strawberries, identifying those that are ripe and placing them in a container [3]. In addition, there is another lettuce harvesting robot developed by the Japanese company in Kyoto called Spread, which can harvest up to 30,000 heads of lettuce per day [4]. This robot uses cameras and sensors to identify ripe lettuce, cut it, and sort it according to quality. These advances demonstrate how technology designed to explore space can also have a significant impact on agriculture and other industries here on Earth.



Figure 2. Agrobot, robot with artificial intelligence to identify and select ripe strawberries. Source: [3].

In particular, rovers can become valuable tools in what is called precision agriculture (PA). PA is an advanced agricultural technique that leverages technology to manage crops by observing, measuring, and responding to the variability of factors that affect the agricultural cycle. Not only can this technique increase productivity and reduce production costs, but it also contributes significantly to reducing the environmental impact of agriculture by minimizing the use of pesticides and other chemicals [5].

Agriculture represents a fundamental pillar of the Peruvian economy, as can be seen in Figure 3. In this context, technological development becomes a key element to enhance the positive impact of the agricultural sector. The Peruvian Ministry of Agriculture and Irrigation highlights that AP has emerged as a fundamental tool to increase agricultural

efficiency and productivity [6]. Indeed, the implementation of the Chavimochic–Olmos Project and the promotion of agro-export agriculture on the Peruvian coast have catalyzed remarkable agricultural progress. Particularly noteworthy is the use of drones or RAPs to carry out precise topographic surveys, as well as the use of thermal and spectral cameras to identify water stress, measure nitrogen content in plants, and detect pests and diseases early. These technological advances not only improve the efficiency of the sector but also contribute significantly to the sustainability and continued growth of Peruvian agriculture.

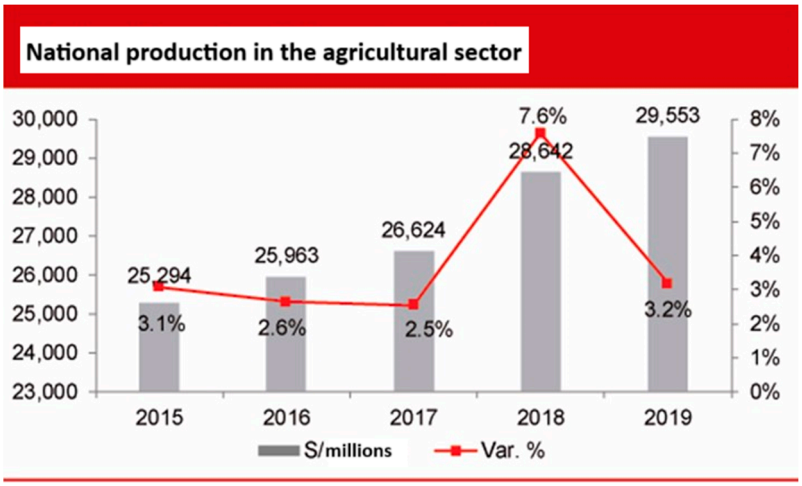


Figure 3. According to figures from the National Institute of Statistics and Informatics (INEI), in 2019, the agricultural sector was 5.4% of the total GDP in 2019. Source: [7].

Internationally, precision agriculture is becoming increasingly crucial due to the growing global demand for food. According to United Nations projections, the world's population is expected to reach 8.5 billion by 2030, representing a 60% increase in global food demand [8]. PA is presented as a fundamental tool to address this challenge as it has the potential to significantly improve agricultural efficiency and productivity, while minimizing its environmental impact [9].

Given the relevance of technological progress in agriculture, it is interesting and important to analyze the applicability of rovers in this sector, taking advantage of their favorable characteristics. One of the most crucial aspects of these devices is their suspension system, which justifies a thorough analysis. There are several suspension system options for agricultural rovers [10]. However, there is still room for improvement in these systems [11,12]. This is timely since the application of mobile robotic systems in agriculture is a developing field [13].

Particularly, the rocker–bogie suspension system has some disadvantages such as the high weight of the mechanism, low operating speed, and difficulty in controlling the orientation of the rover's wingspan [14]. In addition, it is common to test rover suspension system designs experimentally to verify theoretical results [15,16]. However, this practice may result in a waste of money and time resources. In summary, it is necessary to carry out structural and dynamic analysis through numerical simulations in order to optimize the rocker–bogie suspension system when applied in common agricultural terrains, which in turn allows maximizing the efficiency and functionality of the rovers in this context.

2. Fundamentals of Rover Static Analysis

2.1. Rocker–Bogie Suspension Characteristics

The rocker–bogie suspension is a passive articulation design commonly employed on Mars rovers and rovers to overcome obstacles in rough terrain due to its stability and

adaptability [17]. This system basically consists of two main parts that join together and have freedom of rotation: the rocker and the bogie (Figure 4).

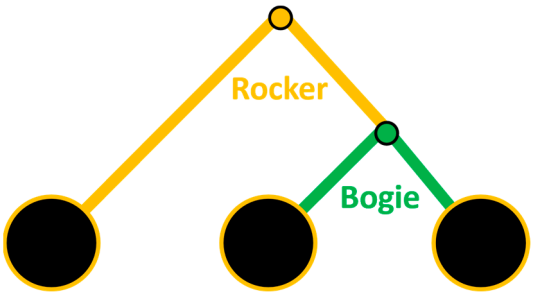


Figure 4. Distinction of the main parts of the rocker–bogie mechanism seen from one side of the vehicle. Own elaboration.

One end of the rocker houses a driving wheel while a bogie element that can pivot on the rocker is attached to the other end [18]. At both ends of the bogie element is a driving wheel, thus there are six wheels in total on the mechanism, three on each side of the rover [19].

We now proceed to further detail this suspension system, its operation and some salient features with the aid of Figure 5.

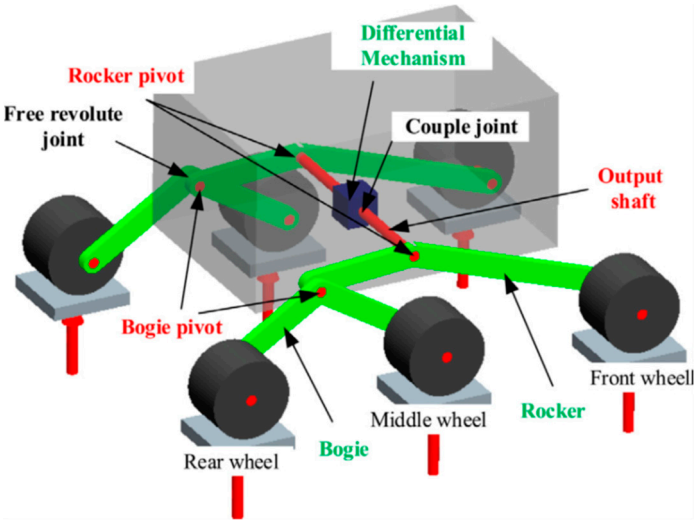


Figure 5. Complete view of the suspension system and its elements. Source: [20].

- The rocker is attached to the rover body by a differential mechanism so that when one rocker goes upward with respect to the chassis, the other goes downward. The chassis is maintained at an average angle between the two rockers [21].
- The rocker–bogie design does not incorporate springs or axles per wheel, allowing the rover to overcome obstacles such as rocks larger than twice the diameter of the wheels while keeping all six wheels on the ground [22].
- During travel, this type of suspension maintains equal load distribution on all wheels and avoids a low frequency of oscillation. [21].
- As with any suspension system, tilt stability is limited by the height of the center of gravity [23].

2.2. Rocker and Bogie Geometric Parameters

Figure 6 shows in detail all the parameters that define the geometrical design of the rocker–bogie suspension. Some important relationships between certain geometric parameters are shown below:

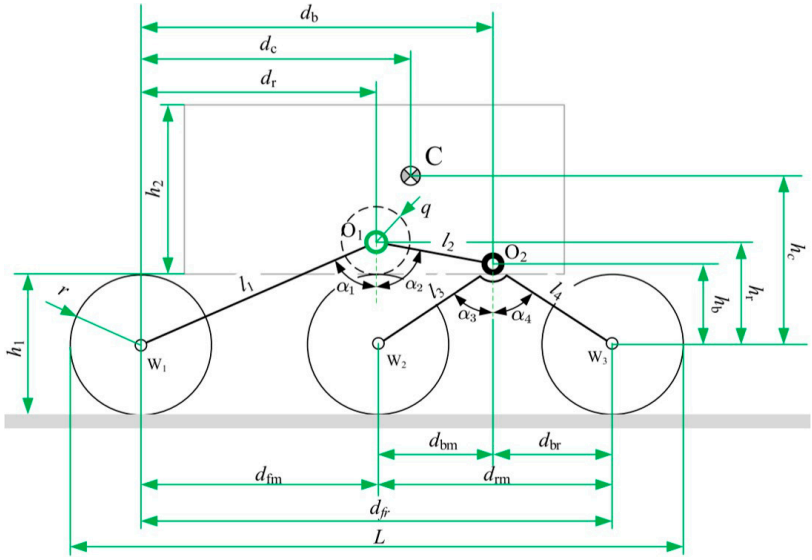


Figure 6. Geometric parameters of a rocker–bogie suspension. Source: [20].

- Rocker lengths (l_1 and l_2): Affect the distance between the front and rear wheels. It should be long enough to keep the wheels in contact with the ground even on steep slopes. A longer rocker provides greater stability but may also increase the overall length of the rover. They are calculated as follows:

$$l_1 = \sqrt{{d_{fm}}^2 + {h_r}^2} \tag{1}$$

$$l_2 = \sqrt{{d_{bm}}^2 + (h_r - h_b)^2} \tag{2}$$

- Bogie lengths (l_3 and l_4): These determine the distance between the two sides of the rover. They should allow enough flexibility to negotiate obstacles without losing traction. A longer bogie allows more flexibility on uneven terrain. They are calculated as follows:

$$l_3 = \sqrt{{d_{bm}}^2 + {h_b}^2} \tag{3}$$

$$l_4 = \sqrt{{d_{br}}^2 + {h_b}^2} \tag{4}$$

- Rocker angle (θ_r): An optimum angle provides a good load distribution between the wheels. It is obtained by the following:

$$\theta_r = \alpha_1 + \alpha_2 \tag{5}$$

- Bogie angle (θ_b): This affects lateral stability and ability to negotiate rocks. It is obtained by the following:

$$\theta_b = \alpha_3 + \alpha_4 \tag{6}$$

- Tilt angle (α): The angle between the rover and the horizontal.

NOTE: Equations (1)–(6) were easily found from the geometric relationships seen in Figure 6.

2.3. Static Analysis

2.3.1. Equilibrium Conditions

To analyze the rover in a state of rest, focusing particularly on its suspension system, one can resort to the conditions of equilibrium of a rigid body, which state that if the resulting force and moment are zero, the rigid body is in equilibrium [24].

$$F_R = \sum F = 0 \tag{7}$$

$$(M_R)_o = \sum M_o = 0 \tag{8}$$

Equation (7) denotes the translational equilibrium of the rigid body, while Equation (8) refers to the rotational equilibrium; both are derived from Newton's first law. From those general equations, six equations can be derived that can be applied to rigid bodies in equilibrium [25]. In this way, the suspension mechanism will be used to analyze each of its components.

$$\sum F_x = 0 \quad \sum F_y = 0 \quad \sum F_z = 0 \tag{9}$$

$$\sum M_x = 0 \quad \sum M_y = 0 \quad \sum M_z = 0 \tag{10}$$

2.3.2. Safety Factor

Before performing the stress and deformation calculation, it is necessary to establish the safety factor in order to evaluate and validate the geometry of the rocker–bogie suspension in terms of structural strength. The factor of safety is a multiplicative factor applied to the resistance of a mechanical component to ensure its safety and reliability under applied loads and depends on the uncertainty associated with the loads, resistance, and behavior of the component [26]. An insufficient safety factor can lead to the premature failure of a component, while an excessive safety factor can result in an oversized and costly component [27].

Ríos and Roncancio [28] and Hernandez et al. [29] describe the Pugsley criterion, which states that the factor of safety (η_s) results from multiplying two coefficients as shown in Equation (11). These coefficients depend on some of the design characteristics specified in Table 1.

$$\eta_s = \eta_{sx}\eta_{sy} \tag{11}$$

where

η_{sx}: safety coefficient involving characteristics A, B, and C.
η_{sy}: safety coefficient involving characteristics D and E.

Table 1. Description of the design features considered to evaluate the safety factor. Table based on [28].

Characteristic	Description
A	Quality of materials, workmanship, maintenance, and inspection
B	Control over the load applied to the part
C	Accuracy of stress analysis, experimental data, or experience with similar devices
D	Danger to personnel
E	Economic impact on the consequences of design

Tables 2 and 3 are used to obtain the values of η_{sx} and η_{sy}, respectively, according to certain considerations based on Pugsley's criteria. Thus, features A, B, and C are identified

by the symbols: very good (mb), good (b), fair (r), and poor (p). Meanwhile, characteristics D and E are identified with the following symbols: very serious (ms), serious (s), and not serious (ns).

Table 2. Values of η_{sx} as a result of combining conditions A, B, and C. Source: [28,29].

Characteristics		B =			
		mb	b	r	p
A = mb	C = mb	1.1	1.3	1.5	1.7
	C = b	1.2	1.45	1.7	1.95
	C = r	1.3	1.6	1.9	2.2
	C = p	1.4	1.75	2.1	2.45
A = b	C = mb	1.3	1.55	1.8	2.05
	C = b	1.45	1.75	2.05	2.35
	C = r	1.6	1.95	2.3	2.65
	C = p	1.75	2.15	2.55	2.95
A = r	C = mb	1.5	1.8	2.1	2.4
	C = b	1.7	2.05	2.4	2.75
	C = r	1.9	2.3	2.7	3.1
	C = p	2.1	2.55	3.0	3.45
A = p	C = mb	1.7	2.15	2.4	2.75
	C = b	1.95	2.35	2.75	3.15
	C = r	2.2	2.65	3.1	3.55
	C = p	2.45	2.95	3.45	3.95

Table 3. Values of ηsys a result of combining conditions D and E. Source: [28,29].

Characteristics	D =		
	ns	s	ms
E = ns	1.0	1.2	1.4
E = s	1.0	1.3	1.5
E = ms	1.2	1.4	1.6

2.3.3. Young's Modulus and Yield Strength

The material used to build the rover has a yield stress, which is the maximum stress it can withstand without permanent deformation [30]. This limit must be considered when designing the suspension system components. This limit or creep resistance can be identified in Figure 7.

Young's modulus (E) or modulus of elasticity can be established by Equation (12) so that this modulus is the slope of the unit stress–strain curve in the elastic region shown in Figure 7. This relationship is known as Hooke's law:

$$E = \frac{S}{e} \tag{12}$$

where

S: engineering stress, which is defined by Equation (13).

e: engineering deformation, which is defined in Equation (14).

$$S = \frac{F}{A_o} \tag{13}$$

where

F: force.
A_o: original cross-sectional area.

$$e = \frac{\Delta l}{l_o} \tag{14}$$

where

Δl: change in length after the force is applied F.
l_o: original length.

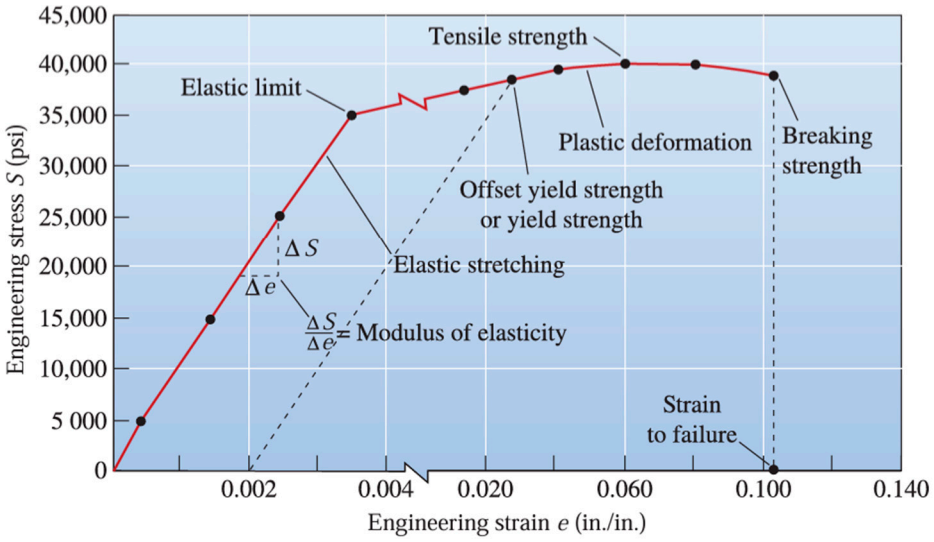


Figure 7. Engineering stress–strain curve of an aluminum alloy. Source: [30].

2.3.4. Stress and Strain

Among the parameters to be evaluated are the stress and strain of the components. Clearly, the obtainment of these variables will be facilitated by means of the software used for the simulation, but it is pertinent to establish what each one refers to and its simplest mathematical conception.

Stress is a physical magnitude that measures the intensity of the internal forces acting on a deformable body [27]. Stress is defined as the force applied over an area as shown in Equation (15).

$$\sigma = \frac{F}{A} \tag{15}$$

where σ is the stress (N/m^2), F is the force (N), and A is the area (m^2).

Strain refers to the change in the size or shape of the structure when loads are applied to a system [31]. In [31], the strain is written as Equation (16).

$$\varepsilon = \ln(l + e) \tag{16}$$

where ε is the strain (m), l is the original length (m), and e is the change of dimension (m).

2.3.5. Von Mises Parameter

The Von Mises creep criterion is based on the basic hypothesis of the distortion energy theory. According to it, when the distortion strain energy for combined stresses equals the maximum elastic distortion energy in single stress, failure will occur [32].

The Von Mises stress is known as an equivalent stress because it is a single value that represents the combined effect of the various loads that a material can experience (from tension and compression to shear, bending, and torsion) [33]. These loads are described by the stress tensor of order three:

$$\begin{matrix} \sigma_{xx} & \sigma_{xy} & \sigma_{xz} \\ \sigma_{yx} & \sigma_{yy} & \sigma_{yz} \\ \sigma_{zx} & \sigma_{zy} & \sigma_{zz} \end{matrix} \quad (17)$$

In this way, the Von Mises stress can be calculated from the components of the tensor shown in Expression (17) [33].

$$\sigma_v = \sqrt{\frac{(\sigma_{xx} - \sigma_{yy})^2 + (\sigma_{yy} - \sigma_{zz})^2 + (\sigma_{zz} - \sigma_{xx})^2 + 6(\sigma_{xy}{}^2 + \sigma_{yz}{}^2 + \sigma_{zx}{}^2)}{2}} \quad (18)$$

In addition, the Von Mises parameter at a point of a deformable solid can be easily calculated from the principal stresses of the tensor shown in Expression (19) according to Equation (20) [33].

$$\begin{matrix} \sigma_1 & 0 & 0 \\ 0 & \sigma_2 & 0 \\ 0 & 0 & \sigma_3 \end{matrix} \quad (19)$$

$$\sqrt{\sigma_v} = \sqrt{\frac{(\sigma_1 - \sigma_2)^2 + (\sigma_2 - \sigma_3)^2 + (\sigma_3 - \sigma_1)^2}{2}} \quad (20)$$

The Von Mises parameter, then, is a fundamental tool in mechanics of materials since it is used to predict the creep of materials under complex loads from uniaxial tensile test results. This parameter is commonly used for ductile materials such as metals.

2.4. Ansys, the Analysis Tool

Ansys is a finite element analysis (FEA) software developed by Ansys, Inc. (Canonsburg, PA, USA). It is a powerful tool that can be used to analyze a wide range of engineering problems, including the static analysis of components [34].

2.4.1. General Characteristics

The following are some general features of Ansys that describe this program and justify its wide use in various engineering fields [35].

- Support for a wide range of materials and properties: Ansys can model a wide range of materials, including metals, polymers, composites, ceramics, and fluids. It can also model nonlinear materials, such as composites and viscoelastic materials.
- Complex geometry modeling: Ansys can model complex geometries, including curved surfaces, compound solids, and non-continuous surfaces.
- Advanced solution methods: Ansys uses a variety of advanced solution methods to solve finite element problems, including the Galerkin finite element method, the generalized Galerkin finite element method, and the flow domain finite element method [36].

- Results visualization and analysis: Ansys provides powerful results visualization and analysis tools that allow users to visualize analysis results and perform post-processing analysis. An example is shown in Figure 8.

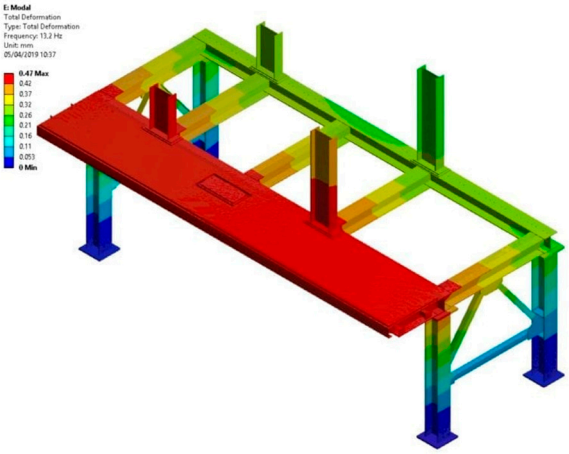


Figure 8. Visualization and obtaining results in an Ansys static analysis. Source: [37].

2.4.2. Static Analysis Techniques of Components in Ansys

Static component analysis is a type of finite element analysis used to determine the stresses, strains, and displacements of a component under static loads [38]. In Ansys, static component analysis can be performed using the Static Structural module. This module provides a variety of static analysis techniques, including the following:

- Linear static analysis: This type of analysis is used for components that meet the linearity conditions.
- Non-linear static analysis: This type of analysis is used for components that do not meet the linearity conditions.
- Static/dynamic analysis: This type of analysis is used for components that are subject to dynamic loads.

2.4.3. Steps to Perform a Static Component Analysis

The steps followed to perform the analysis are usually somewhat standardized, although, clearly depending on what is being sought, there will be certain variations. In the following, a series of general steps that can be followed to perform the static analysis of components are specified [39,40].

Step 1—Define the geometry of the component: The user must create a CAD model of the component to be analyzed.

Step 2—Assign materials and properties: The user must assign materials and properties to each element of the CAD model.

Step 3—Apply loads and constraints: The user must apply loads and constraints to the CAD model.

Step 4—Solve the model: Ansys will solve the model using the selected finite element method.

Step 5—Visualize and analyze the results: The user can visualize and analyze the results of the analysis using the Ansys results visualization and analysis tools.

3. Static Analysis by Finite Elements

The present study has a fundamentally quantitative approach since the variables involved in the evaluation of the rocker–bogie suspension are of this category. These

variables are certain geometric parameters of the suspension and those that allow evaluating the strength of the system structure, either stresses or deformations.

In addition, the type of research is correlational since it seeks to find the relationships between certain geometric variables of the rocker–bogie suspension and the static resistance variables (stresses and deformations) in order to finally perform an optimization of the geometry of the suspension system evaluated by means of the maximum Von Mises stress. All this parameter evaluation is performed with the help of Ansys (Mechanical) software using certain specific modules.

To fully determine the analysis of this work, it is established that the research design is non-experimental transectional. The research is non-experimental because the response of the suspension system structure is evaluated only by varying the geometry and without manipulating variables such as the applied load, boundary conditions (constraints), the material of the components, among others. Also, it is transectional because the investigation takes place in a specific instant of time.

Thus, it is evident that the unit of analysis is a rover and specifically the rocker–bogie suspension system. The numerical simulations performed in Ansys Mechanical constitute the instrument of analysis of this research by which the results that can occur in reality without the need of long periods of time and the implementation of the rover are approximated. Next, the flow diagram is presented in Figure 9, which summarizes the path followed to develop the study.

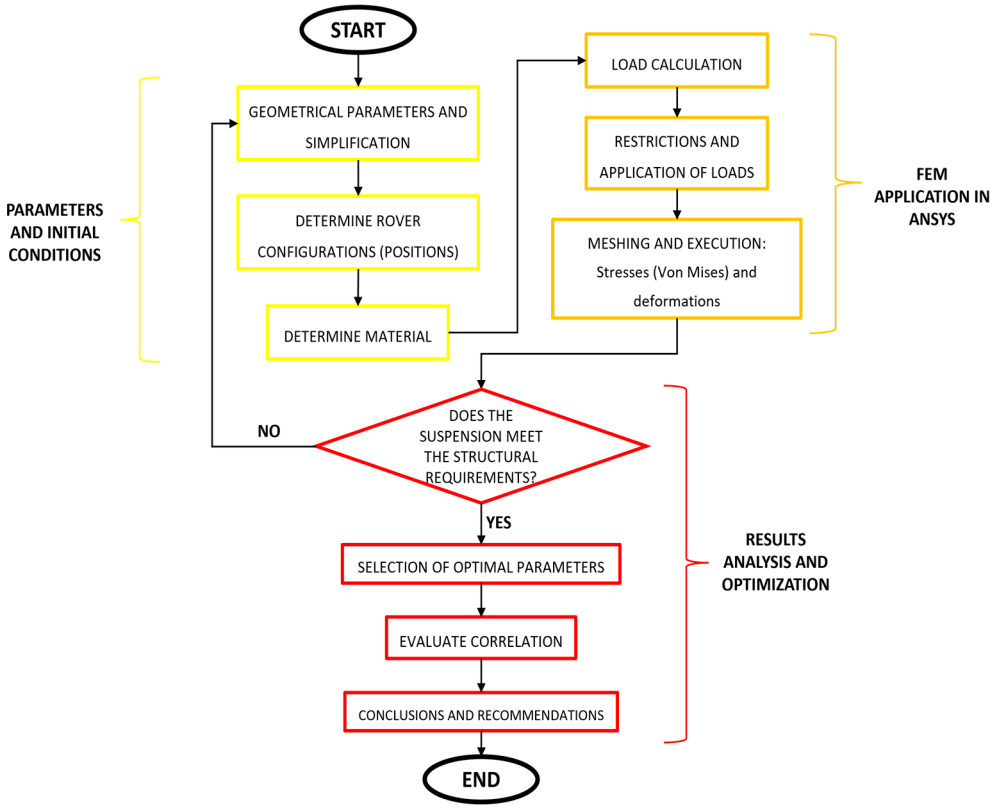


Figure 9. Flow chart of the research stages for obtaining results and optimization. Own elaboration.

3.1. Parameters and Initial Conditions

In principle, we proceeded to simplify the rocker–bogie suspension of a rover design (Figure 10) in order not to make the simulations more difficult and due to the limitations of the Ansys Student 2023 R2 software. It should be noted that a rigid interaction between the ground and the tires is assumed.

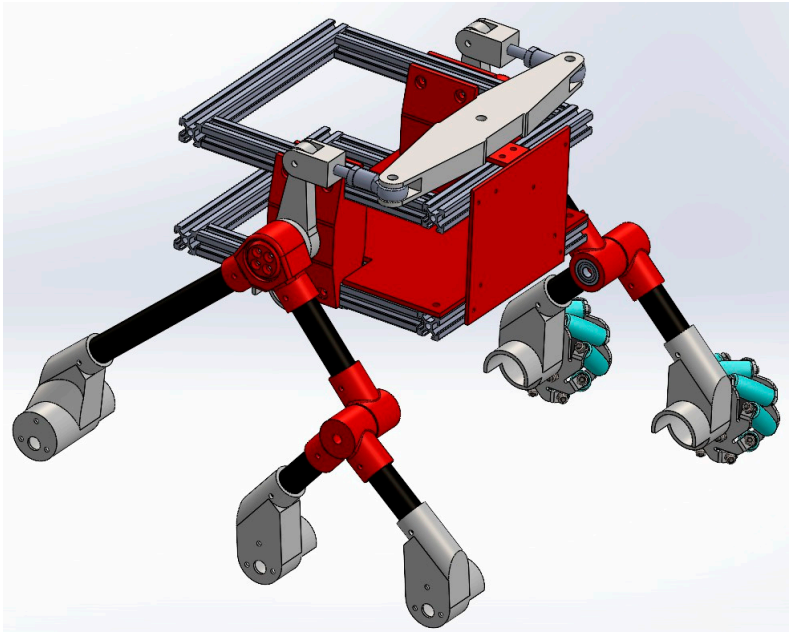


Figure 10. Own design of a rover whose suspension system will be simplified by assumptions and component modifications.

The symmetry of the design allows only one side of the suspension to be evaluated. From there, the simplest geometry that will define the rocker–bogie suspension and its respective geometric parameters is defined. The rocker and bogie are treated as a single element despite the rotating joint between them.

The altitude of the rocker element, the altitude of the bogie element and the largest diagonal of the geometry were assigned as the parameters that will be modified repeatedly to optimize the system taking into account the maximum Von Mises stress and deformations.

Although the rocker and bogie angles can also be modified for optimization, it was decided to leave them as fixed values (Equation (21)).

$$\theta_r = \theta_b = 90^\circ \tag{21}$$

The initial test values of the rocker element altitude, bogie element altitude, and largest diagonal are as follows:

$$h_r = 150 \text{ mm} \tag{22}$$

$$h_b = 70 \text{ mm} \tag{23}$$

$$l_2 + l_4 = 300 \text{ mm} \tag{24}$$

These would be the main geometrical parameters; the others are automatically calculated and adjusted thanks to the design software (DesignModeler 2023 R2) of Ansys and are based on the relationships shown in the fundamentals of Section 2.

With the base geometry, a simplified profile of the rocker element was designed with certain similar characteristics. With this profile and a thickness of 20 mm, the rocker element was obtained. The bogie element was designed in the same way.

With the 3D design of the elements as one, the suspension could be evaluated in different configurations (positions) such as when crossing an obstacle, as shown in Figure 11. Thanks to the visual aid of this figure, it is worth mentioning here that the design of the suspension geometry will also be limited by the size of the wheels. Therefore, it should be noted that the designed rover will have 80 mm diameter wheels.

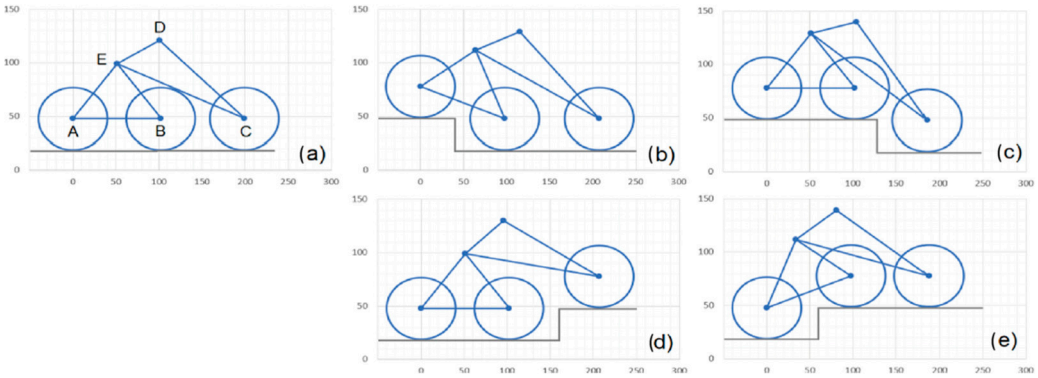
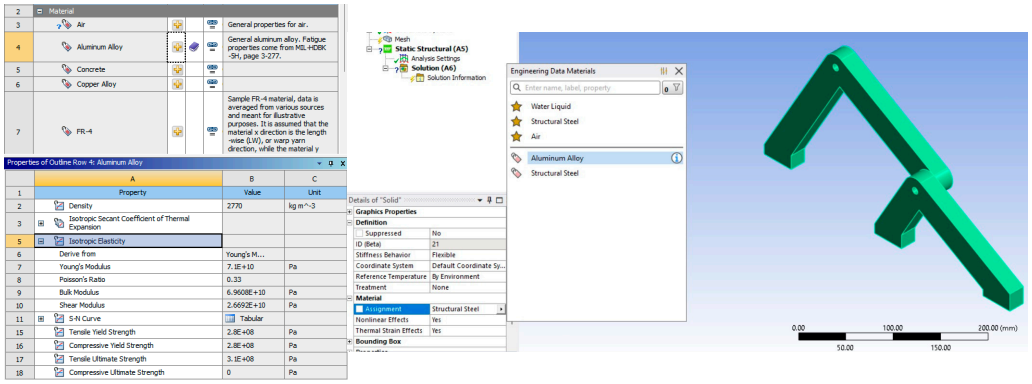


Figure 11. Different configurations of a rover along a run. (**a**) Rover on flat surface; (**b**) Front wheels above the obstacle; (**c**) Front and middle wheels above the obstacle; (**d**) Rear wheels above the obstacle; (**e**) Middle and rear wheels above the obstacle. Source: [41].

However, the study will only consider the simplest configuration shown in Figure 11a, which occurs when the rover is on a flat surface.

Thus, the final 3D design of the structure will be analyzed as a single piece and in the desired configuration. The design had to be adapted to simplify the application of constraints and loads and to try to replicate certain features of the original design.

As a final part of this configuration of parameters and initial conditions, we proceeded with the choice of the material of the elements. Therefore, it is necessary to add the aluminum alloy and its properties to the Static Structural module where the simulation will be performed as shown in Figure 12.



(**a**) (**b**)

Figure 12. Configuration of the structure material. (**a**) Mechanical properties of aluminum alloy; (**b**) assignment of the material to the 3D solid of the Static Structural module.

3.2. FEM Application in Ansys Mechanical

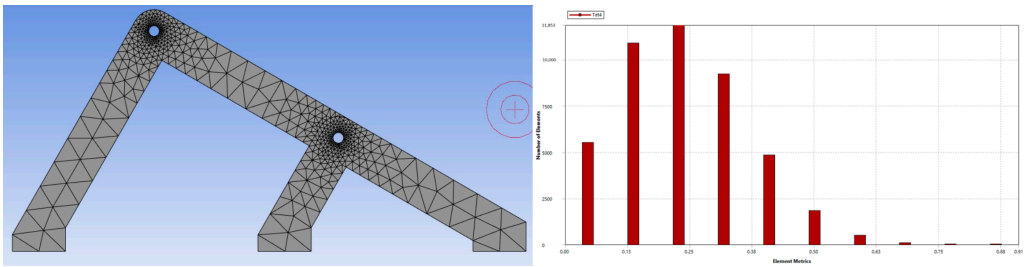
In [29], the total load exerted by the chassis and payload on a rover is estimated to be 60 N. By symmetry, such force is distributed over the two sides of the rocker–bogie suspension system equally:

$$F = \frac{60}{2} = 30\ N \tag{25}$$

This force will be applied vertically at O_1, a connection hole of the rocker element to the rover chassis. To be more faithful to reality, this load should be considered to be of the Ansys *Bearing Load* type, defined as a bearing load that is applied to a specific surface or interface where the structure is expected to come into contact with another component, such as a bearing, a bearing surface, or any type of interface. Once the force is applied to the suspension structure, some movements must be restricted by means of the fixed

supports that limit the six possible degrees of freedom of a part of the rocker–bogie system. Therefore, the movement of the three ends of the system where the wheels would go is completely restricted.

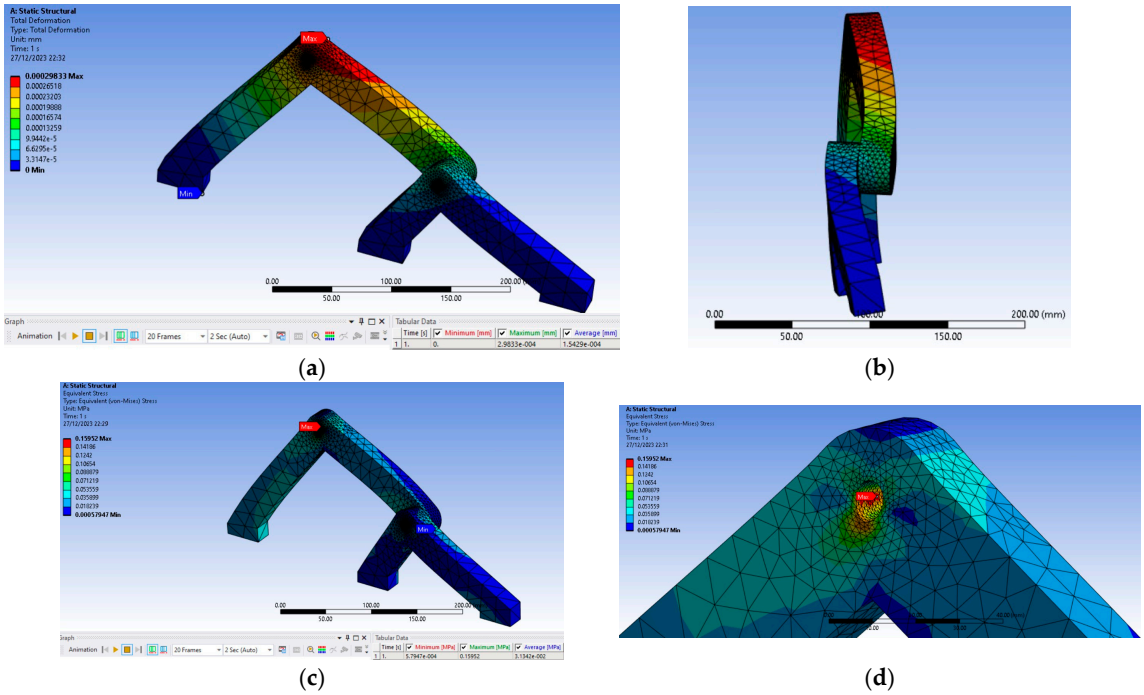
Prior to the execution of the FEM, the CFD type meshing (used in fluid simulations) is performed with its predetermined parameters, and the discretization is also validated by means of the *Skewness* metric. Conveniently, a smaller mesh size is noticeable in the cylindrical parts or joints due to the curvature. The Skewness metric allows us to say that the meshing is adequate because a greater number of elements are on the left side of the graph shown in Figure 13b, which means a division of the structure into smaller elements, which in turn will allow a better approximation of the results.



(**a**) (**b**)

Figure 13. CFD meshing of the rocker–bogie system. (**a**) Front view of the CFD meshing of the rocker–bogie system; (**b**) histogram of division "elements" size. Trend to the left side.

Then, finite element analysis can be applied to find the required results according to the configuration shown in Figure 14a.



(**a**) (**b**)

(**c**) (**d**)

Figure 14. Execution and results of the simulation: deformations and Von Mises stresses. (**a**) Results of the deformations in the structure where the positions of the maximum and minimum values are indicated; (**b**) exaggerated lateral view of the deformations occurring in the suspension structure; (**c**) results of the Von Mises stresses in the structure where the positions of the maximum and minimum values are indicated; (**d**) close-up of stress concentration at the connection of the rocker arm to the chassis.

A similar stress concentration would occur at the connection between the rocker and bogie. In this simulation, this is not observed since the whole structure is a single body since it was not performed as an assembly.

3.3. Results Analysis and Optimization

In order to perform multiple simulations quickly and proceed with parameter optimization, the project schematic was configured in the Ansys environment. The range in which the input (independent) variables vary must be limited as shown in the following figures. Geometry constraints, e.g., wheel size, must be taken into account here.

With the experiment designer, the table shown in Figure 15 shows the input variables (3 geometric parameters) and the output variable (maximum Von Mises stress).

Table of Outline A2: Design Points of Design of Experiments

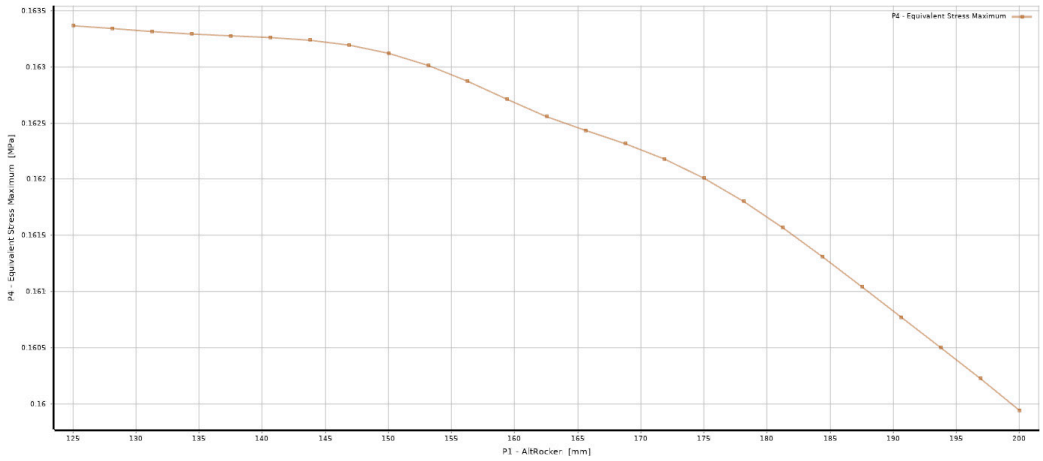
	A	B	C	D	E
1	Name	P1 - AltRocker (mm)	P2 - AltBogie (mm)	P3 - LargRocker (mm)	P4 - Equivalent Stress Maximum (MPa)
2	1	162.5	75	300	0.16256
3	2	125	75	300	0.16337
4	3	200	75	300	0.15994
5	4	162.5	50	300	0.16245
6	5	162.5	100	300	0.16693
7	6	162.5	75	250	0.18184
8	7	162.5	75	350	0.16099
9	8	132.01	54.674	259.35	0.16155
10	9	192.99	54.674	259.35	0.15396
11	10	132.01	95.326	259.35	0.16385
12	11	192.99	95.326	259.35	0.15486
13	12	132.01	54.674	340.65	0.15669
14	13	192.99	54.674	340.65	0.15526
15	14	132.01	95.326	340.65	0.16536
16	15	192.99	95.326	340.65	0.17059

Figure 15. Limits of variation of the largest diagonal.

The behavior of the target variable as a function of the input variables is shown in Figure 16 in different graphs.

- The maximum equivalent stress decreases as the rocker height increases.
- In general, the maximum equivalent stress increases as the bogie height increases within its range of variation.
- In general, the maximum equivalent stress decreases as the largest diagonal increases within its range of variation.

It is also possible to obtain 3D plots of the behavior of the maximum equivalent stress as a function of two geometric variables as shown in Figure 17.



(**a**)

Figure 16. *Cont.*

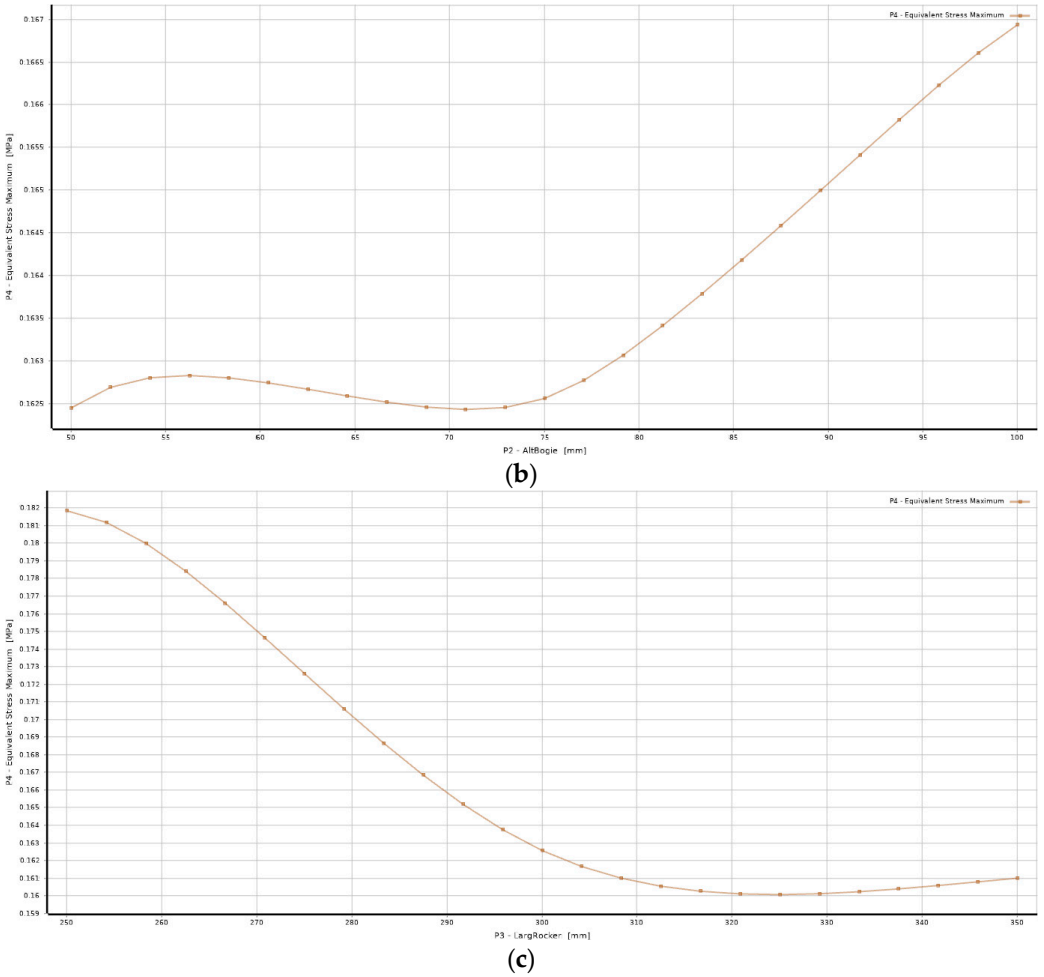


Figure 16. Behavior of maximum equivalent stress as a function of the input variables. (**a**) Maximum equivalent stress as a function of rocker height; (**b**) maximum equivalent stress as a function of bogie height; (**c**) maximum equivalent stress as a function of the largest diagonal.

These plots are used to identify correlation patterns between the variables and, therefore, will serve to parameterize and delimit the optimization settings. In the graphs, it should be identified for which values of the geometrical parameters the minimum and maximum equivalent maximum stresses occur. The table of experiments also serves the same purpose.

With this information, multiple tests can be performed to find and verify, for example, a target value of maximum Von Mises stress. The most obvious would be to look for the minimum value of the output variable within all the tests or experiments performed. However, one should also evaluate the stress distribution across the geometry and take into account the deformations.

To check the optimization by inspection and multiple tests, you can also use ***Optimization*** from the ***Response Surface Optimization*** module. The optimization process being searched for is configured.

Although a maximum equivalent stress of 0.16 MPa was sought, a different result is obtained in Figure 18. This is because the optimization is based on statistical methods without considering the physics of the system.

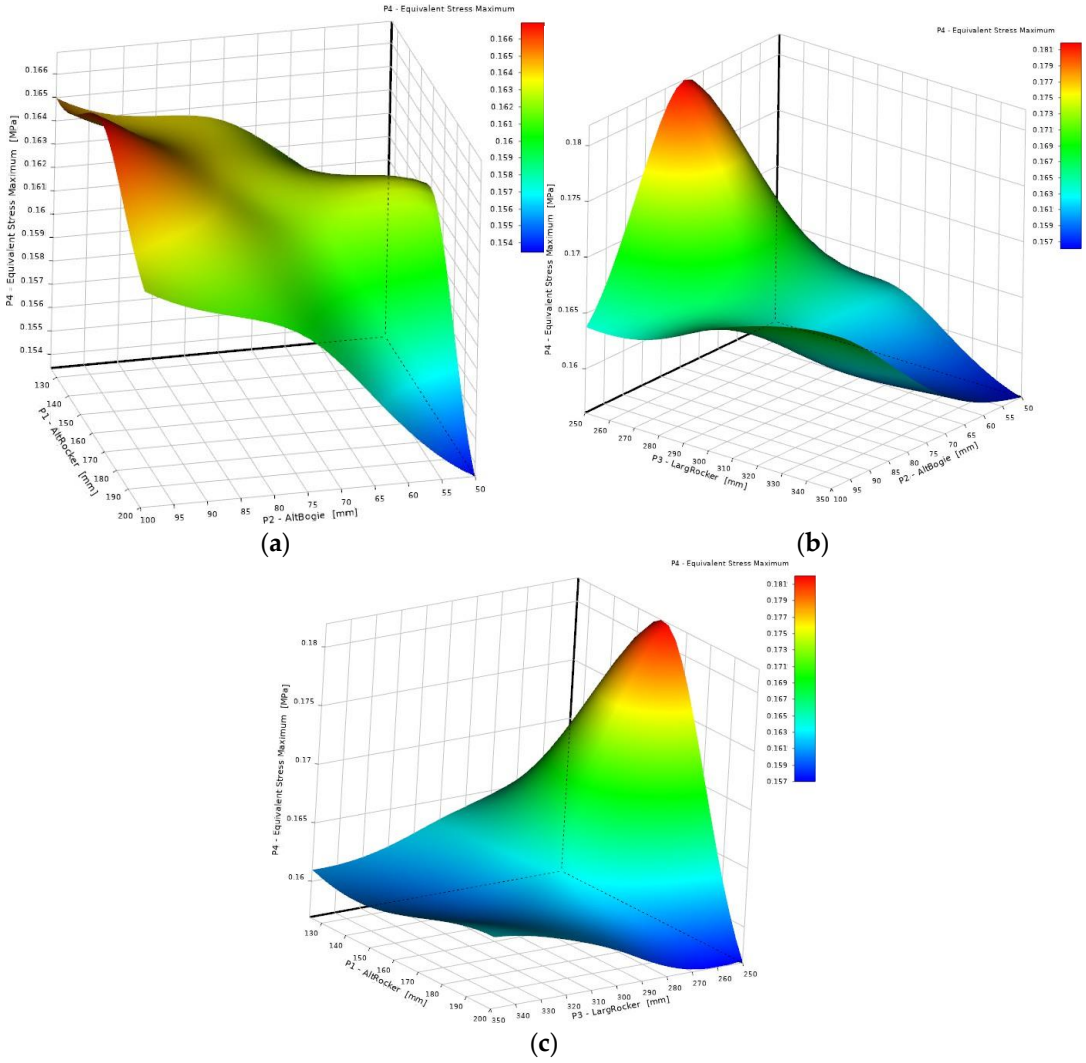


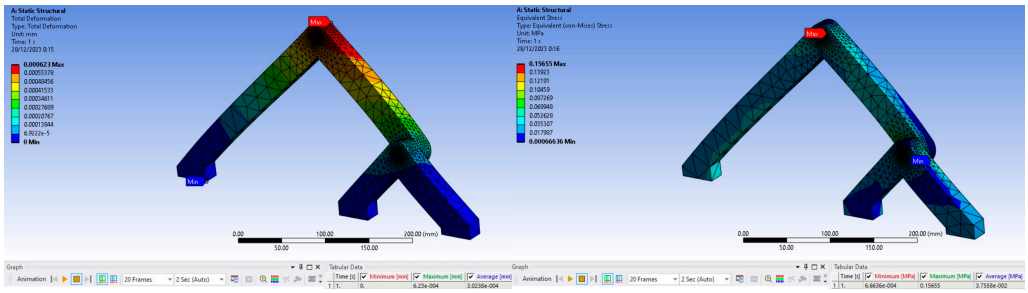
Figure 17. Behavior of maximum equivalent stress as a function of 2 input variables. (**a**) Maximum equivalent stress as a function of rocker and bogie heights; (**b**) maximum equivalent stress as a function of bogie height and largest diagonal; (**c**) maximum equivalent stress as a function of rocker height and largest diagonal.

Table of Design Points

	A	B	C	D	E	F	G	H
1	Name	P1 - AltRocker	P2 - AltBogie	P3 - LargRocker	P4 - Equivalent Stress Maximum	Retain	Retained Data	Note
2	Units	mm	mm	mm	MPa			
3	DP 0 (Current)	191.76	71.641	281.94	0.15655	☑	✓	
*						☐		

Figure 18. Updating of the geometric parameter values resulting from the optimization.

However, after performing multiple simulations, the geometric parameters shown in Figure 18 were determined as the optimal ones for this case study considering maximum stress, stress distribution, deformations, and geometric constraints (such as wheel size or geometry incoherence). The simulation applying the optimal parameters and the resulting stress concentration at the connection of the rocker arm to the chassis are shown in Figure 19 and Figure 20 respectively.



(**a**) (**b**)

Figure 19. Deformations and Von Mises stresses results the optimized structure. (**a**) Deformation (or strain) results of the optimized structure. Maximum and minimum deformation are shown; (**b**) Von Mises stress result in the optimized structure. Maximum and minimum equivalent stresses are shown.

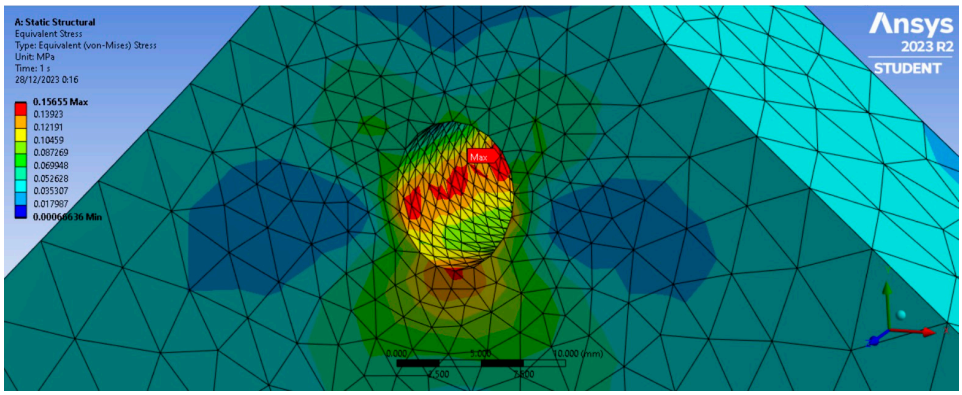
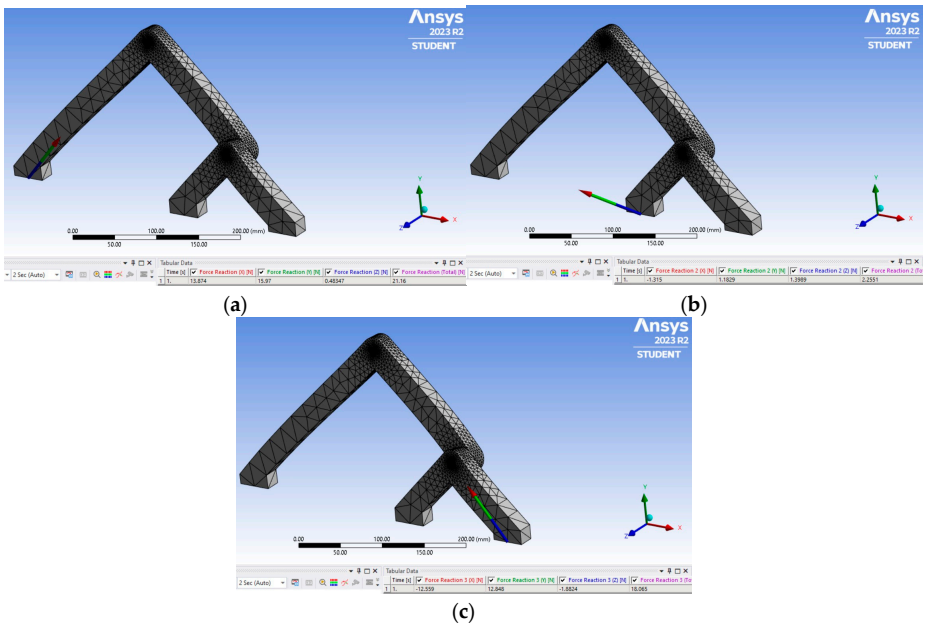


Figure 20. Stress concentration at the rocker and chassis joints. Stress symmetry is observed.

It is also possible to obtain the values of the reactions at the soil contacts as shown in Figure 21.



(**a**) (**b**)

(**c**)

Figure 21. Reaction forces on fixed supports after optimization. (**a**) Reaction force on fixed support 1; (**b**) reaction force on fixed support 2; (**c**) reaction force on fixed support 3.

3.4. Dynamics Simulation

Finally, to validate the geometry obtained by the optimization through FEM analysis, one can also opt for a dynamic simulation to observe the performance of the rover during its movement on irregular surfaces. For this purpose, Facci and Arra [42] provide a simulation environment where the dynamic model of a six-wheeled rover with a rocker–bogie suspension system is used in addition to proposing a position and velocity control system using PID controllers. They also provide the facility to analyze different images to obtain a profile of the terrain that the rover will have to travel.

This simulation environment was developed in MATLAB R2023b and Simulink and can be easily adapted to the model proposed in this work. Thus, by taking a default terrain profile and modifying variables such as the gravity (the original code defaults to Mars gravity), mass, and rover geometry parameters shown in Figure 18, it was possible to observe the performance of the proposed rover on an irregular surface.

From Figure 22, it is evident that the rover can overcome this terrain profile, showing very small errors in velocity and position tracking, as well as little control effort to achieve it.

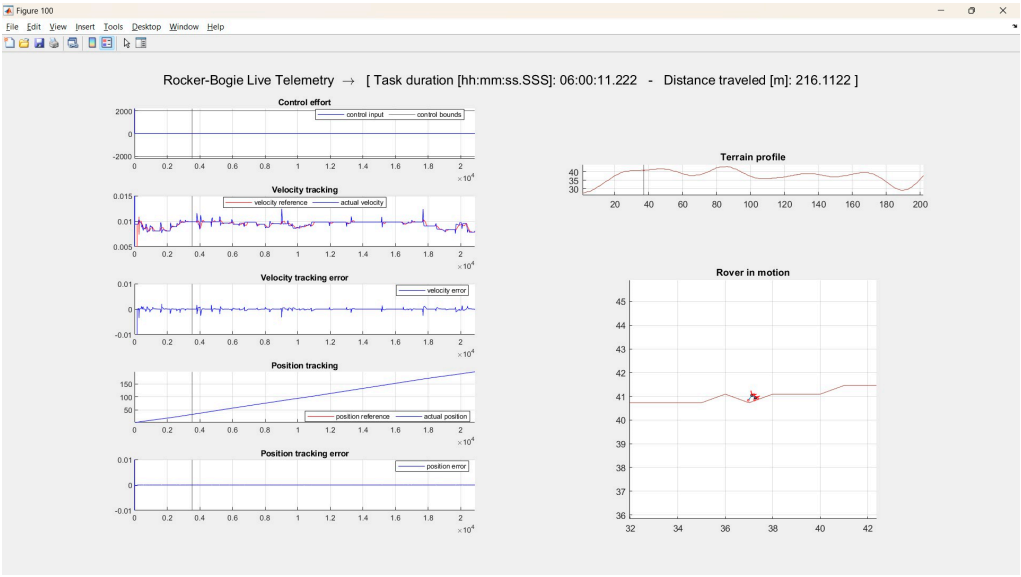


Figure 22. Dynamic simulation of the rocker–bogie suspension, showing the tracking of the position and velocity on an irregular surface.

4. Conclusions and Recommendations

Using geometric simplifications and physical assumptions, the geometry of the rocker–bogie suspension system was optimized through numerical simulations with ANSYS Student, which employs the finite element method. Variations were made in key geometric parameters, such as the altitude of the rocker and bogie elements, as well as the maximum diagonal length; and the target variable considered was the maximum Von Mises stress. This optimized suspension design will be implemented as an integral part of a rover structure intended for PA.

During static analysis and testing, the various relationships between the input variables and the output variable were explored, observing trends and patterns of behavior. This exploration, supported by numerical and graphical data, played a crucial role in the optimization process. The relationships were evaluated not only in two dimensions (independent variable–dependent variable) but also in three dimensions (independent variables–dependent variable), allowing a more global analysis of the parameters.

It is important to note that, since the efforts are concentrated on the rocker, bogie, and chassis connections, it is recommended to reinforce these specific areas to prevent possible structural failures. This strengthening will significantly contribute to improve the performance of the rover throughout its lifetime, ensuring its structural strength and its ability to face challenges during its tasks.

In terms of recommendations, it is suggested to improve the meshing of the elements and to consider the maximum deformation as an additional variable of interest. In addition, it is proposed to develop a more realistic model that considers the assembly and connections, thus allowing a more accurate approximation of the results and facilitating a more effective optimization of the geometric parameters.

To perform a more exhaustive analysis of the rocker–bogie suspension system, we propose the variation of parameters that have been considered constant until now, such as rocker and bogie angles, applied load, rover configuration, and thickness, among others. By considering these factors as variables, not only will optimization be improved, but also other key aspects of rover performance, such as the maximum load it can support, can be determined.

Finally, although a dynamic simulation of the proposed model was performed to validate the good performance of the rover during its trajectory, it is recommended to complement the results obtained in this study with a more exhaustive dynamic analysis, e.g., a dynamic optimization. This will allow the adjustment of the rocker–bogie suspension geometry to achieve efficient mechanical strength, increased stability, and more favorable obstacle overcoming. In sum, these approaches have the potential to optimize the robustness of the proposed autonomous rover suspension system, tailoring it to the specific needs of the PA.

Author Contributions: Conceptualization, L.L.; methodology, N.M.R. and L.L.; software, L.L.; validation, N.M.R.; formal analysis, L.L. and N.M.R.; investigation, L.L.; resources, L.L. and N.M.R.; data curation, L.L.; writing—original draft preparation, L.L. and N.M.R.; writing—review and editing, L.L. and N.M.R.; visualization, L.L.; supervision, N.M.R.; project administration, L.L. All authors have read and agreed to the published version of the manuscript.

Funding: This research received no external funding.

Institutional Review Board Statement: Not applicable.

Informed Consent Statement: Not applicable.

Data Availability Statement: Data available on request due to restrictions.

Conflicts of Interest: The authors declare no conflict of interest.

References

1. El Universo. *La Historia de Todos los Robots Exploradores de la NASA en Marte*; El Universo: Guayaquil, Ecuador, 2021.
2. Milo, A. Perseverance, el vehículo robotizado que busca vida en Marte. *National Geographic en Español*, 25 October 2023.
3. Kardoudi, O. Las nuevas máquinas que sustituirán a los agricultores y jornaleros. *El Confidencial*, 15 June 2021.
4. Ruiz García, L. Los 8 Mejores Robots Agrícolas para Huertos pequeños y grandes. *AgroHuerto*, 5 August 2020.
5. Agbar Agriculture. *¿Por qué es tan Importante la Agricultura de Precisión?* Agbar Agriculture: Corduba, Spain, 2021.
6. Instituto Nacional de Innovación Agraria (INIA). Agricultura de Precisión y su Implementación en la Agricultura Peruana. 2019. Available online: https://www.inia.gob.pe/events/cvirtual-2019-precision/ (accessed on 8 December 2023).
7. ComexPerú. Sector agro generó un 4.8% de ingresos tributarios adicionales en el periodo enero-setiembre de 2020 vs. el mismo periodo de 2019. *ComexPerú*, 27 November 2020.
8. United Nations. *World Population Prospects 2019: Highlights*; Number ST/ESA/SER.A/423; United Nations, Department of Economic and Social Affairs, Population Division: New York, NY, USA, 2019.
9. Rastros. La importancia de la agricultura de precisión. *Rastros*, 8 March 2019.

10. Archila, J.F.; Moreira, J.M.; Halts, V.I.V.; Alves, L.A.N.; Rueda, O.E.; Becker, M. Simulation of Rovers for Precision Agriculture. In Proceedings of the 2014 Joint Conference on Robotics: SBR-LARS Robotics Symposium and Robocontrol, Sao Carlos, Brazil, 18–23 October 2014; pp. 229–234. [CrossRef]
11. Brooks, T.; Gold, G.; Sertic, N. *Dark Rover Rocker-Bogie Optimization Design*; Executive Summary; University of British Columbia Library: Vancouver, BC, Canada, 2011.
12. Senjaliya, H.; Gajjar, P.; Vaghasiya, B.; Shah, P.; Gujarati, P. Optimization of Rocker-Bogie Mechanism using Heuristic Approaches. *arXiv* **2022**, arXiv:2209.06927.
13. Califano, F.; Cosenza, C.; Niola, V.; Savino, S. Multibody Model for the Design of a Rover for Agricultural Applications: A Preliminary Study. *Machines* **2022**, *10*, 235. [CrossRef]
14. Wang, S.; Li, Y. Dynamic Rocker-Bogie: Kinematical Analysis in a High-Speed Traversal Stability Enhancement. *Int. J. Aerosp. Eng.* **2016**, *2016*, 5181097. [CrossRef]
15. Cosenza, C.; Niola, V.; Pagano, S.; Savino, S. Theoretical study on a modified rocker-bogie suspension for robotic rovers. *Robotica* **2023**, *41*, 2915–2940. [CrossRef]
16. Choi, D.; Oh, J.; Kim, J. Analysis method of climbing stairs with the rocker-bogie mechanism. *J. Mech. Sci. Technol.* **2013**, *27*, 2783–2788. [CrossRef]
17. Toha, S.F.; Zainol, Z. *System Modelling of Rocker-Bogie Mechanism for Disaster Relief*; Elsevier B.V.: Amsterdam, The Netherlands, 2015; Volume 76, pp. 243–249. [CrossRef]
18. Rantanen, O. Design and Control of a Wall-Driving Rocker-Bogie Robot. Master of Science Thesis, Tampere University, Tampere, Finland, 2019.
19. Miller, D.P.; Lee, T.L. High-Speed Traversal of Rough Terrain Using a Rocker-Bogie Mobility System. In Proceedings of the Robotics 2002: The 5th International Conference and Exposition on Robotics for Challenging Situations and Environments, Albuquerque, NM, USA, 17–21 March 2002.
20. Zheng, J.; Gao, H.; Yuan, B.; Liu, Z.; Yu, H.; Ding, L.; Deng, Z. Design and terramechanics analysis of a Mars rover utilising active suspension. *Mech. Mach. Theory* **2018**, *128*, 125–149. [CrossRef]
21. Mathis-Ullrich, F.; Göktogan, A.H.; Sukkarieh, S. Design Optimization of a Mars Rover's Rocker-Bogie Mechanism using Genetic Algorithms. In Proceedings of the 10th Australian Space Science Conference, Brisbane, Australia, 27–30 September 2010; pp. 199–210.
22. Montaleza, C.; Mayorga, X.; Gallegos, J.; León, R. Diseño de un prototipo de robot con geometría Rocker-Bogie. *Enfoque UTE* **2022**, *13*, 82–96. [CrossRef]
23. Noble, S.; Issac, K.K. An improved formulation for optimizing rocker-bogie suspension rover for climbing steps. *Proc. Inst. Mech. Eng. Part C J. Mech. Eng. Sci.* **2019**, *233*, 6538–6558. [CrossRef]
24. Hibbeler, R.C. *Ingeniería Mecánica—Estática*, 12th ed.; Pearson Educación: London, UK, 2010.
25. Beer, F.P.; Johnston, E.R. *Mecánica Vectorial para Ingenieros*, 11th ed.; McGraw-Hill Education: New York, NY, USA, 2016.
26. Budynas, R.G.; Nisbett, K.J. *Diseño en Ingeniería Mecánica de Shigley*, 9th ed.; Mcgraw-Hill Interamericana De España S.L.: New York, NY, USA, 2012.
27. Beer, F.P.; Johnston, E.R.; DeWolf, J.T.; Mazurek, D.F. *Mecánica de Materiales*, 7th ed.; McGraw-Hill Education: New York, NY, USA, 2017.
28. Ríos Quiroga, L.C.; Roncancio, H.E. Análisis y desarrollo de un programa de selección rápida de factores de seguridad, para diseño de elementos mecánicos. *Sci. Tech.* **2007**, *13*, 255–260.
29. Hernandez Rincón, D.M.; Luque Londoño, D.; Ardila Ordúz, J.A. *Diseño y Construcción de un Vehículo Autónomo Tipo Rover*; Universidad San Buenaventura, Facultad de Ingeniería, Programas de Mecatrónica-Electrónica: Ternera, Colombia, 2005.
30. Askeland, D.R.; Wright, W.D. *The Science and Engineering of Materials*, 6th ed.; Cengage Learning: Boston, MA, USA, 2011.
31. Seralathan, S.; Bagga, A.; Ganesan, U.K.; Hariram, V.; Premkumar, T.M.; Padmanabhan, S. *Static Structural Analysis of Wheel Chair Using a Rocker Bogie Mechanism*; Elsevier Ltd.: Amsterdam, The Netherlands, 2020; Volume 33, pp. 3583–3590. [CrossRef]
32. Popov, E.P.; Balan, T.A. *Mecánica de Sólidos*, 2nd ed.; Pearson Educación: London, UK, 2000.
33. Thompson, E. What Is Equivalent Stress? Blog Post. 2023. Available online: https://www.ansys.com/blog/what-is-equivalent-stress (accessed on 5 December 2023).
34. ANSYS. *Ansys Mechanical*; Ansys: Canonsburg, PA, USA, 2023.
35. Moreno, P.A.; Pérez, A.S. *Método de los Elementos Finitos: Introducción a Ansys*; Universidad de Sevilla: Seville, Spain, 2004.
36. Moaveni, S. *Finite Element Analysis: Theory and Application with ANSYS*; Prentice Hall: Hoboken, New Jersey, USA, 1999.
37. Ingenieria SAMAT. *Utilidad Cálculos ANSYS (III) Evitar Errores Estructurales*; Ingenieria SAMAT: Zaragoza, Spain, 2019.
38. Logan, D.L. *A First Course in the Finite Element Method*, 6th ed.; Un libro de texto completo para los cursos de Elementos Finitos en Ingeniería; Cengage Learning: Stamford, CT, USA, 2016.
39. Madenci, E.; Guven, I. *The Finite Element Method and Applications in Engineering Using ANSYS*; Springer Book: Berlin/Heidelberg, Germany, 2015.

40. Duinto, D. Guía Completa de Análisis de Elementos Finitos con Ansys. Available online: https://duinto.com/guia-completa-de-analisis-de-elementos-finitos-con-ansys/ (accessed on 5 December 2023).
41. Nicolella, A.; Niola, V.; Pagano, S.; Savino, S.; Spirto, M. *An Overview on the Kinematic Analysis of the Rocker-Bogie Suspension for Six Wheeled Rovers Approaching an Obstacle*; Springer Science and Business Media B.V.: Berlin/Heidelberg, Germany, 2022; Volume 122, pp. 86–93. [CrossRef]
42. Facci, M.; Arra, G.S. *Dynamics and Control of a Six-Wheeled Rover with Rocker-Bogie Suspension System*; Dipartimento di Ingegneria Informatica, Automatica e Gestionale: Rome, Italy, 2022.

Disclaimer/Publisher's Note: The statements, opinions and data contained in all publications are solely those of the individual author(s) and contributor(s) and not of MDPI and/or the editor(s). MDPI and/or the editor(s) disclaim responsibility for any injury to people or property resulting from any ideas, methods, instructions or products referred to in the content.